

M22: A [Fe/H] Abundance Range Revealed¹

G. S. Da Costa¹, E. V. Held², I. Saviane³, and M. Gullieuszik²

ABSTRACT

Intermediate resolution spectra at the Ca II triplet have been obtained for 55 candidate red giants in the field of the globular cluster M22 with the VLT/FORS2 instrument. Spectra were also obtained for a number of red giants in standard globular clusters to provide a calibration of the observed line strengths with overall abundance [Fe/H]. For the 41 M22 member stars that lie within the $V - V_{HB}$ bounds of the calibration, we find an abundance distribution that is substantially broader than that expected from the observed errors alone. We argue that this broad distribution cannot be the result of differential reddening. Instead we conclude that, as has long been suspected, M22 is similar to ω Cen in having an intrinsic dispersion in heavy element abundance. The observed M22 abundance distribution rises sharply to a peak at $[Fe/H] \approx -1.9$ with a broad tail to higher abundances: the highest abundance star in our sample has $[Fe/H] \approx -1.45$ dex. If the unusual properties of ω Cen have their origin in a scenario in which the cluster is the remnant nucleus of a disrupted dwarf galaxy, then such a scenario likely also applies to M22.

Subject headings: globular clusters: general — globular clusters: individual (M22) — stars: abundances

1. Introduction

Beginning from observations made more than 30 years ago, we now know that the majority, if not all, globular clusters show star-to-star variations in the abundances of the light elements C, N, O, Na, Al and Mg (see, for example, the reviews of Kraft 1994; Gratton et al. 2004, and references therein). The variations are in the sense that relative to ‘normal’ stars in the cluster, carbon and oxygen are depleted while nitrogen is enhanced, and sodium and aluminum are enhanced while magnesium is depleted, in the stars showing the ‘anomalous’ abundances. Together these effects

¹Research School of Astronomy & Astrophysics, The Australian National University, Mt Stromlo Observatory, via Cotter Rd, Weston, ACT 2611, Australia

²Osservatorio Astronomico di Padova, INAF, vicolo dell’Osservatorio 5, I-35122 Padova, Italy

³European Southern Observatory, Casilla 19001, Santiago 19, Chile

¹Based on data collected at the European Southern Observatory, Paranal, Chile, Proposal No. 77.D-0775.

are known as the O-Na anti-correlation. Despite much work, the origin of the abundance anomalies is not well understood though the fact that they are seen on the main sequence in at least some globular clusters points to a process that is intrinsic to the formation of the cluster (e.g., see the discussion in Marcolini et al. 2009).

In general, however, globular clusters are chemically homogeneous when it comes to the abundances of the iron-peak elements, with the limits on any possible internal range in $[\text{Fe}/\text{H}]$ quite stringent. For example, in their detailed analysis of high dispersion spectra of 36, 23 and 28 red giants in the clusters M5, M3 and M13, Kraft & Ivans (2003) list observed standard deviations for the cluster $[\text{Fe}/\text{H}]$ values in the range 0.03–0.08 dex, consistent with that expected from the errors alone. Consequently, any intrinsic abundance spreads must be considerably smaller. Similarly, Da Costa & Armandroff (1990) used their red giant branch photometry to set 3σ upper limits of 0.04–0.09 dex for any intrinsic heavy element abundance range in six southern clusters.

The well-established exception to the lack of $[\text{Fe}/\text{H}]$ variations in individual clusters is the stellar system ω Centauri, the most luminous of the Galaxy’s globular clusters. While the stars in this cluster show the O-Na anti-correlation (Norris & Da Costa 1995a), they also possess a wide range in overall abundance (e.g., Freeman & Rodgers 1975; Norris & Da Costa 1995b; Pancino et al. 2002) with complex distributions of element-to-iron abundance ratios (see Romano et al. 2007, and the references therein). This indicates that ω Cen is a system that has undergone significant chemical evolution. Indeed the nucleosynthetic contributions of Type II and Type Ia supernovae are recognizable in the variations of abundance ratios with $[\text{Fe}/\text{H}]$, as are the contributions of AGB stars (e.g., Norris & Da Costa 1995b; Smith et al. 2000; Pancino et al. 2002). All in all the observations point to a complex chemical history for ω Cen, with star formation likely to have occurred in the cluster over a period of perhaps 2 Gyr (e.g., Stanford et al. 2006).

The differences between ω Cen and other globular clusters has led to the suggestion that ω Cen may have formed in a different way — that it is the nuclear remnant of a dwarf galaxy which has been disrupted by the tidal field of the Milky Way (e.g., Freeman 1993). Bekki & Freeman (2003), for example, have shown that such a process is dynamically plausible. The different environment may then have facilitated additional chemical processes that do not occur in ‘regular’ globular clusters (e.g., Bekki & Norris 2006; Romano et al. 2007).

In this context the location of the globular cluster M54 at the center of the Sagittarius dwarf spheroidal galaxy is particularly relevant. The Sgr dwarf is currently being tidally disrupted by the Galaxy and in a few Gyr or less, M54 will be seen as a halo globular cluster rather than as the central star cluster of a dwarf galaxy (e.g., Da Costa & Armandroff 1995). It is therefore potentially a current day example of what may have been the situation for ω Cen in the distant past. From an abundance point-of-view the situation is complicated because the cluster is superposed on the general Sgr field population, as well as on that of the Sgr nucleus. Bellazzini et al. (2008) have shown that the Sgr nuclear population is metal-rich ($[\text{Fe}/\text{H}] \approx -0.4$) and kinematically distinct from that of M54, which has $[\text{Fe}/\text{H}] \approx -1.5$ dex. Nevertheless Sarajedini & Layden (1995) claimed from

their analysis of the width of the M54 red giant branch in a $(I, V - I)$ color-magnitude diagram that $\sigma([\text{Fe}/\text{H}])_{int} \approx 0.16$ dex in M54. More recently Bellazzini et al. (2008) have obtained Ca II triplet spectroscopy for over 700 red giants in the central M54/Sgr field. They associate ~ 425 stars with M54 and find $\sigma([\text{Fe}/\text{H}])_{int} \approx 0.14$, in good agreement with previous estimates, and an observed range in $[\text{Fe}/\text{H}]$ from -1.8 to -1.1 dex. Thus the case for M54 being the second star cluster after ω Cen to possess an internal range in $[\text{Fe}/\text{H}]$ is strong, but confirmation from an extensive high dispersion spectroscopic study remains to be done. Such a study would also allow measurement of [element/Fe] ratios and their variation (if any) with $[\text{Fe}/\text{H}]$, from which, as for ω Cen, constraints could be placed on the enrichment processes.

The other globular cluster that is often mentioned in the context of ω Cen-like abundance variations, albeit on a smaller scale, is M22 (NGC 6656). Unlike ω Cen and M54 which are both very luminous clusters with $M_V \approx -10.3$ and -10.0 , respectively, M22 is a cluster of bright but not outstanding luminosity, with $M_V \approx -8.5$ (Harris 1996). It lies at low galactic latitude approximately 3 kpc from the Sun and 5 kpc from the Galactic Center (Harris 1996). Based on DDO photometry for 10 M22 red giants, Hesser, Hartwick & McClure (1977) were the first to suggest an analogy between M22 and ω Cen by noting that the observed range of ultraviolet excesses and CN-strengths in their M22 sample was similar to that seen in ω Cen stars (see also Hesser & Harris 1979). This was followed by the much more extensive study of Norris & Freeman (1983), who obtained low resolution spectra for ~ 100 M22 red giants. They reported the existence of a correlation between the strength of cyanogen features and the strength of the Ca II H and K lines in their M22 spectra: such a phenomenon was also seen in similar spectra of ω Cen red giants but was much less marked for red giants in the ‘normal’ cluster NGC 6752. Based on synthetic spectra Norris & Freeman (1983) then went on to conclude that the observed range in calcium line strengths in M22 corresponded to an abundance range $\Delta[\text{Ca}/\text{H}] \approx 0.3$, and that the cluster shared the anomalous abundance patterns of ω Cen, though to a smaller degree.

In the ensuing decades the debate as to whether M22 does or does not share many of the characteristics of ω Cen, particularly as regards the presence of a range in heavy element abundance, has swung back and forth with little consensus and a number of divergent results. The situation is complicated by the clear presence of differential reddening across the field of the cluster: $\Delta E(B - V) \approx 0.06 - 0.08$ mag (e.g., Anthony-Twarog et al. 1995; Monaco et al. 2004). A brief survey of existing results (see Monaco et al. 2004, for additional references) includes the following. Lehnert et al. (1991) used spectra at Ca II triplet region of 10 red giants to conclude that M22 was similar to ω Cen in displaying Ca, Na and Fe abundance variations. They estimated $\Delta[\text{Ca}/\text{H}] \sim \Delta[\text{Fe}/\text{H}] \sim 0.4$ dex, a result similar to that of Norris & Freeman (1983). On the other hand, Anthony-Twarog et al. (1995) concluded from Stromgren+Ca photometry of ~ 300 red giants and horizontal branch stars that there was no evidence for a range in $[\text{Fe}/\text{H}]$ in the cluster. Monaco et al. (2004) reached similar conclusions from their extensive wide-field photometry of M22: the maximum metallicity spread permitted by their data is $\Delta[\text{Fe}/\text{H}] \sim 0.1 - 0.2$ dex (Monaco et al. 2004). Further, Ivans et al. (2004), using high dispersion spectra for 26 M22 red giants, were able to find a consistent set of

spectroscopic and chemical constraints which gave acceptable stellar parameters and no requirement for any variations in $[\text{Fe}_{\text{II}}/\text{H}]$.

Most recently, Marino et al. (2009) analyzed high dispersion UVES spectra for 17 red giants, and lower resolution GIRAFFE spectra for 14 stars, in the cluster. In addition to the O-Na anti-correlation that is also seen in many clusters, they identified the presence of two groups of stars whose mean abundances for the *s*-process elements Y, Zr and Ba differ by ~ 0.6 dex. The *s*-process rich group also appears to have higher iron and calcium abundances by 0.14 ± 0.03 and 0.25 ± 0.04 dex, respectively (Marino et al. 2009). In this context it is also worth noting that Piotto (2009) has presented a HST-based color-magnitude diagram for M22 in which it is evident that there are two distinct cluster sub-giant branches. M22 thus joins other clusters such as ω Cen, NGC 2808 and NGC 1851 where such diagrams provide evidence for the presence of two or more internal cluster populations that have different properties (see Piotto 2009, and references therein).

As part of a larger program to study Galactic globular clusters with uncertain abundance determinations, we have investigated the question of an abundance spread in M22 anew, by obtaining intermediate resolution spectra at the Ca II triplet of a substantial number of M22 red giant stars. Ca II triplet line strength measurement from such spectra is a well established technique for determining overall abundances (e.g., Armandroff & Da Costa 1991; Rutledge et al. 1997b; Battaglia et al. 2008). In §2 the observations and reductions are described, while in §3 a calibration of the measured line strength indices with overall abundance is generated. The results for M22 are also presented in §3 and are discussed in §4. In brief, we find strong evidence that there is an overall abundance spread in our M22 sample of size similar to that originally found by Norris & Freeman (1983) and Lehnert et al. (1991), and consistent with the results of Marino et al. (2009). Moreover, the M22 abundance distribution bears some similarity to that for ω Cen, although on a reduced scale.

2. Observations and Reductions

2.1. Observations

Short and ‘long’ exposures of each cluster in the program were first obtained in service time with the FORS2 instrument in imaging mode at the Cassegrain focus of the VLT-UT1 telescope, primarily to define the targets for spectroscopic follow-up. The $6.8' \times 6.8'$ field-of-view was centered on the cluster for the sparser or more distant systems, but was offset from the centers for the nearer and richer clusters, including the ‘standard’ clusters. These latter clusters were taken from the compilation of Pritzl et al. (2005) and possess well established $[\text{Fe}/\text{H}]$ values (e.g. Kraft & Ivans 2003) that cover the full range of metallicities exhibited by Galactic globular clusters. Observation of such clusters in addition to the program clusters allows the derivation of a line strength – abundance calibration from the subsequent spectroscopic observations. The images were obtained in the *V* and *I* bands.

Point-Spread-Function photometry was carried out on both the long and short exposure pairs using Stetson’s DAOPHOT/ALLSTAR package (Stetson 1987, 1994). The resulting instrumental magnitudes were then provisionally calibrated by using color terms, which are small, and zero points provided by ESO as part of their routine quality control². Color-magnitude (c-m) diagrams were then generated to allow the selection of likely cluster members as targets for the spectroscopic observations. They also permit characterization of the principal c-m diagram features, such as horizontal-branch morphology. We note though that for the clusters considered here, superior photometric data are available from other sources, for example from Monaco et al. (2004) for M22. The calibration approach adopted means that the photometry is likely to be consistent with the standard V, I system, but that the zero points for each cluster data set are uncertain at the 0.05–0.10 mag level. However, since our analysis uses only *differential* magnitudes, such as the magnitude difference from the horizontal branch, the zero point uncertainty is not a concern. We note that for each cluster the data sets from the two detectors in the camera were treated separately: stars falling on CCD1 are labeled as ‘1.’ followed by a running number and those falling on CCD2 as ‘2.’ (cf. Tables 1,2).

The spectroscopic observations were then carried out in visitor mode with the FORS2 instrument in MOS-mode during a two night run at the end of May in 2006. Conditions on the first night were photometric while on the second night there was intermittent thick cloud. On both nights the seeing was quite variable, from below 1'' to worse than 2''. The instrument was used with the 1028z+29 grism and the OG590+32 order-blocking filter. This gives a maximum spectral coverage of $\sim 7700\text{\AA} - 9500\text{\AA}$ at a scale of 0.85 \AA per (binned) pixel. The allocation of targets to slits was done in such a way that the wavelength interval $\sim 8200\text{\AA} - 8900\text{\AA}$ was always on the detector. The number of stars observed in each cluster per configuration varied from ~ 10 to the maximum of 19, depending on the density of likely members within the field-of-view. The magnitude range was set as ~ 3 mag (or somewhat less) to insure sufficient coverage of the red giant branch, and the exposure times were chosen to ensure the brightest stars were close to, but not saturated. Two exposures were obtained to allow removal of cosmic-rays. For the majority of clusters only single configurations were used, but for M22 three separate configurations were observed to increase the sample size. The M22 field was centered to the east of the cluster center (see Fig. 5).

2.2. Reductions

All spectra were extracted using the FORS2 pipeline version 1.2 (Izzo & Larsen 2008), and in particular the FORS_CALIB and FORS_SCIENCE pipeline recipes were used to wavelength calibrate and extract the spectra. The first recipe takes as input the master bias frame, the screen flat-field frames and the arc frame, and computes the wavelength calibration and distortion map for each slit, after finding the slit positions. A catalog of arc lines and a grism parameter table, part of the

²see www.eso.org/observing/dfo/quality/FORS2/qc/photcoeff/photcoeffs_fors2.html

package, are also given as input. The mean residual in the wavelength calibration was 0.24 pixels, the mean spectral resolution was $R \approx 2440$, and the mean FWHM of the arc lines was $3.51 \pm 0.07 \text{ \AA}$.

Once the calibration tables were created, they were used with the FORS_SCIENCE recipe to reduce the target spectra. This recipe cannot process multiple exposures simultaneously, so each frame was reduced independently, and then the two exposures were average-combined. The software corrects for bias and flatfield, and computes a local sky background for each slit, to be subtracted from the object spectra. Cosmic-ray rejection was not applied. The extraction radius was 6 pix, and Horne optimal extraction was applied (Horne 1986). The spectra were normalized by exposure time, and the wavelength solution was aligned to a reference set of >20 sky lines by applying an offset. The median offset was 0.9 pix. The final product of the pipeline is then a FITS cube containing the fully reduced spectra. Each object is identified by its position and extraction window in the rectified spectrum, and by the row number in the FITS cube holding the reduced spectra. To associate each spectrum to the corresponding target star, the spatial transformation between the ‘rectified CCD’ coordinates of the slitlets and the original target coordinates were computed. In this way it was easy to verify that the objects detected in each slitlet corresponded to the expected target. Finally a table was created, where for each star the J2000 coordinates, the V and I magnitudes, and the name of the associated spectrum are given.

The S/N ratios for the final spectra varied from ~ 110 for the brightest stars to ~ 25 for the faintest in a typical exposure. In Fig. 1 we show examples of the final spectra for a star in NGC 6397, two stars in M22, and one star in M10. All four stars have $V - V_{HB} \approx -0.5 \text{ mag}$.

3. Analysis

The first step in the analysis of the reduced spectra for each cluster was measurement of the individual radial velocities. This was carried out with the RVIDLINES task in IRAF’s RV package using all three of the Ca II triplet lines. After heliocentric correction the individual velocities were compared with the cluster radial velocity from the compilation of Harris (1996). Obvious outliers were discarded as definite non-members and the remaining velocities averaged. For the 5 standard clusters (M15, NGC 6397, M10, M4 and M71), the mean difference between the cluster velocities determined here and that tabulated by Harris (1996) was $0 \pm 3 \text{ km s}^{-1}$, where the uncertainty is the standard error of the mean.

3.1. Abundance Calibration

For the radial velocity member stars in the standard clusters the (pseudo) equivalent widths of the $\lambda 8542\text{\AA}$ and $\lambda 8662\text{\AA}$ lines of the Ca II triplet were measured by fitting gaussian line profiles using the feature and continuum bands listed in Armandroff & Da Costa (1991). Along with the value, the fit also returns an uncertainty in the measured equivalent width. The sum of the

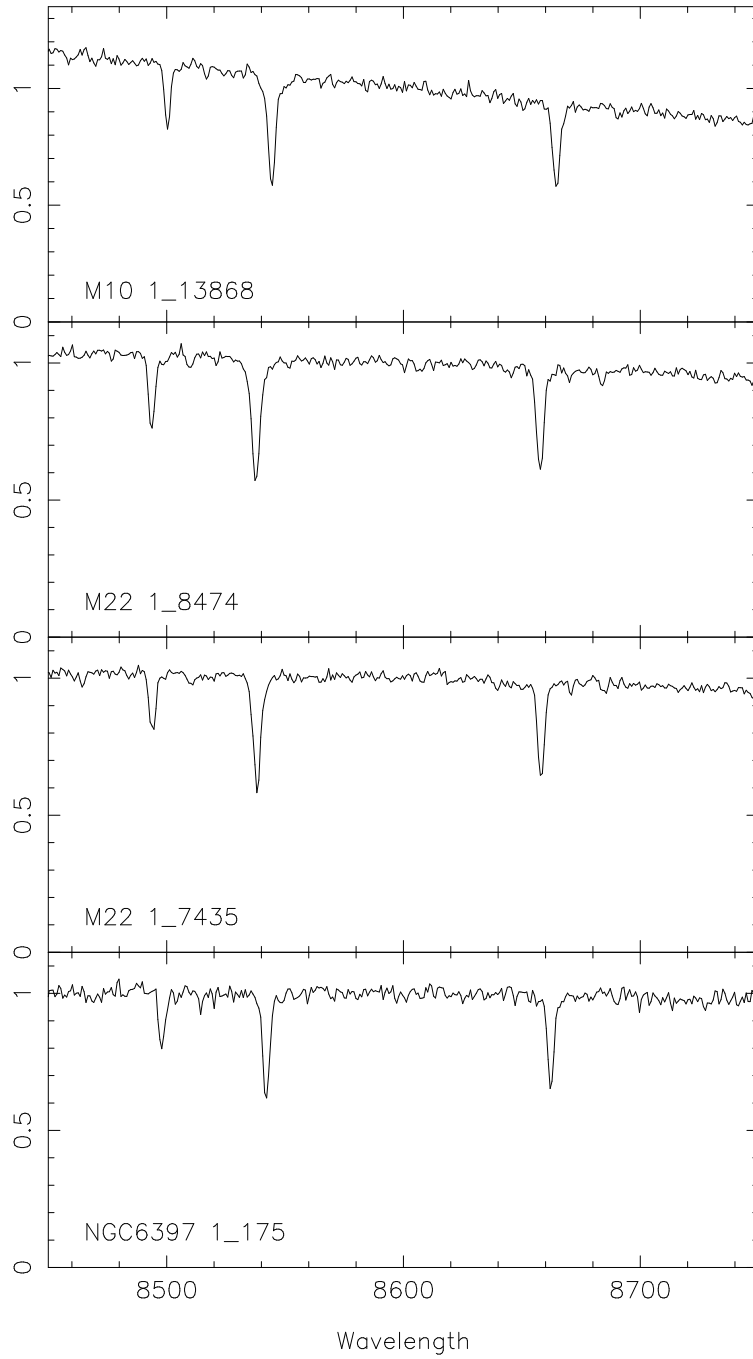


Fig. 1.— Example spectra from the clusters NGC6397, M22 and M10. All 4 stars have approximately the same $V-V_{HB}$ value. The spectra have been normalized at $\lambda \approx 8600\text{\AA}$ but have not otherwise been altered from those used in the analysis.

two measurements, $W_{8542} + W_{8662}$, was then plotted against the magnitude difference from the horizontal branch, $V - V_{HB}$, with the measurement uncertainty in $W_{8542} + W_{8662}$ taken as the quadratic combination of the uncertainties for the two lines. For all clusters the V values come directly from the photometry of the FORS2 imaging observations with the V_{HB} values determined from the color-magnitude diagrams generated with those photometry sets. As noted above, the CCD1 and CCD2 sets were treated separately though in practice the two V_{HB} values generally agreed well. Three M71 stars, and one NGC 6397 star, lay off the $(W_{8542} + W_{8662}, V - V_{HB})$ relations defined by the other cluster stars; we assumed these stars are non-members. Given that both M71 and NGC 6397 have relatively low radial velocities, the fact that velocity is an imperfect membership discriminator is not surprising.

To increase the number of standard clusters available to establish the abundance calibration, the standard cluster observations from Gullieuszik et al. (2009) were also analysed. These spectra were obtained with the identical instrument setup and were reduced using the same methods as employed here. The clusters observed were NGC 4590, NGC 4372, NGC 6397 (no stars in common with our data set), NGC 6752, M5 and NGC 6171. The line strengths on these spectra were measured in an identical fashion to those for the standard clusters observed here. The $V - V_{HB}$ values were taken from Gullieuszik et al. (2009).

For each of the 10 standard clusters, the $(W_{8542} + W_{8662}, V - V_{HB})$ data were fit with a straight line via least squares. The dependence of the resulting slopes on abundance was investigated and found to be negligible. A weighted average of the slopes was then formed and the resulting single value of $-0.51 \pm 0.01 \text{ \AA/mag}$ refitted to the data for each cluster. The results of this process are shown in Fig. 2. Two points are worth noting. First, as is visible in Fig. 2 in the data for NGC 6397 and to a lesser extent for M10, the slope of the $(W_{8542} + W_{8662}, V - V_{HB})$ relation appears to notably flatten for $V - V_{HB}$ values greater than approximately $+0.2 \text{ mag}$. Consequently, in the analysis here and subsequently, only stars with $V - V_{HB}$ less than $+0.2$ are considered. Second, the slope derived here is larger than the values near -0.64 \AA/mag found in other studies (e.g., Armandroff & Da Costa 1991; Rutledge et al. 1997a; Battaglia et al. 2008; Gullieuszik et al. 2009). Our explanation for this difference is the following. Because of the somewhat higher resolution of these spectra compared to those of Armandroff & Da Costa (1991) for example, the gaussian-only fitting technique employed here underestimates the contribution to the pseudo-equivalent widths from the line profile wings, with this underestimate being larger for stronger lines (see Battaglia et al. 2008, for similar comments). We have investigated this through a comparison of the $W_{8542} + W_{8662}$ values measured here with those of Gullieuszik et al. (2009), who used a ‘gaussian + lorentzian’ measurement technique that includes the contribution from the line wings. The comparison shows an excellent correlation over the full range of measured values for the 41 stars in 6 clusters in common. However, the $W_{8542} + W_{8662}$ values of Gullieuszik et al. (2009) are 17% stronger, and when coupled with the 0.51 \AA/mag slope found here, predicts that Gullieuszik et al. (2009) should see a slope of 0.60 \AA/mag for their relation between $W_{8542} + W_{8662}$ and $V - V_{HB}$. Gullieuszik et al. (2009) actually determine a slope of $0.63 \pm 0.02 \text{ \AA/mag}$. Thus our explanation

for the smaller slope found here is likely the correct one. However, since there is no dependence of the fitted slope on abundance, and since the range of $V - V_{HB}$ values covered is similar for most of the clusters, our use of the slope determined here should not affect any of the results. In particular, we note that if we consider only stars in the standard clusters with $V - V_{HB} < -0.5$, rather than $< +0.2$, then the weighted mean slope found is $-0.54 \pm 0.02 \text{ \AA/mag}$. This value is not significantly different from that adopted and indicates that our choice of a limit at $V - V_{HB} = 0.2$ for stars to include in the abundance calibration process does not unduly influence the results.

The variation of $W_{8542} + W_{8662}$ with $V - V_{HB}$ can then be removed by calculating the value of the reduced equivalent width W' , where W' is the mean value of $W_{8542} + W_{8662} + 0.51(V - V_{HB})$ for the stars in each cluster, subject to the condition that $V - V_{HB} \leq 0.2$ where necessary. This single parameter W' then needs to be calibrated with some other measure of cluster abundance. In most situations the calibration is made to overall abundance, designated by $[\text{Fe}/\text{H}]$, with the $[\text{Fe}/\text{H}]$ values chosen from other compilations. Armandroff & Da Costa (1991) adopted the $[\text{Fe}/\text{H}]$ scale of Zinn & West (1984) while others, for example Rutledge et al. (1997b) and Battaglia et al. (2008), have provided calibrations to the $[\text{Fe}/\text{H}]$ scale of Carretta & Gratton (1997). Kraft & Ivans (2003) have derived a new $[\text{Fe}/\text{H}]$ scale for globular cluster abundances by consistently analyzing high-dispersion spectra for a number of red giants in 16 key clusters with $-2.4 \leq [\text{Fe}/\text{H}] \leq -0.7$ dex. In their study Kraft & Ivans (2003) consider the effects of different model atmospheres and different color-temperature relations. Here we adopt their $[\text{Fe}/\text{H}]$ values based on the MARCS model atmospheres as our fundamental calibration points. As Kraft & Ivans (2003) note, these abundances are generally about 0.2 dex lower than those of Carretta & Gratton (1997).

Fig. 3 shows the relation between W' and $[\text{Fe}/\text{H}]_{\text{MARCS}}$ from Kraft & Ivans (2003) for our 10 standard clusters. Over the range of $[\text{Fe}/\text{H}]_{\text{MARCS}}$ shown, the relation is linear with no indication of any change in slope towards the higher metallicities. We defer to a subsequent paper the question of the calibration for clusters that exceed the abundance of M71, the most metal-rich cluster included here. The error bars for the W' values come from the dispersion of the $W_{8542} + W_{8662}$ values about the fitted slope (cf. Fig. 2) while the errors in the $[\text{Fe}/\text{H}]_{\text{MARCS}}$ values are taken from the discussion in the Appendix of Kraft & Ivans (2003). A linear regression applied to the points in Fig. 3 yields the equation:

$$[\text{Fe}/\text{H}]_{\text{MARCS}} = (0.549 \pm 0.031) \times W' - (3.369 \pm 0.102) \quad (1)$$

The rms dispersion about the fitted line is 0.092 dex which is consistent with the average uncertainty of the $[\text{Fe}/\text{H}]_{\text{MARCS}}$ values (Kraft & Ivans 2003), and we adopt this relation as our calibration to overall abundance. To within the uncertainties our calibration relation is identical to that, namely:

$$[\text{Fe}/\text{H}]_{\text{MARCS}} = (0.531 \pm 0.025) \times W' - (3.279 \pm 0.086) \quad (2)$$

given by Kraft & Ivans (2003) for the relation between $[\text{Fe}/\text{H}]_{\text{MARCS}}$ and the W' values of Rutledge et al. (1997a).

The data for the standard cluster stars observed here are given in Table 1. In successive columns we list the cluster and star ID, the RA and dec, the heliocentric velocity, the value of $V - V_{HB}$ and

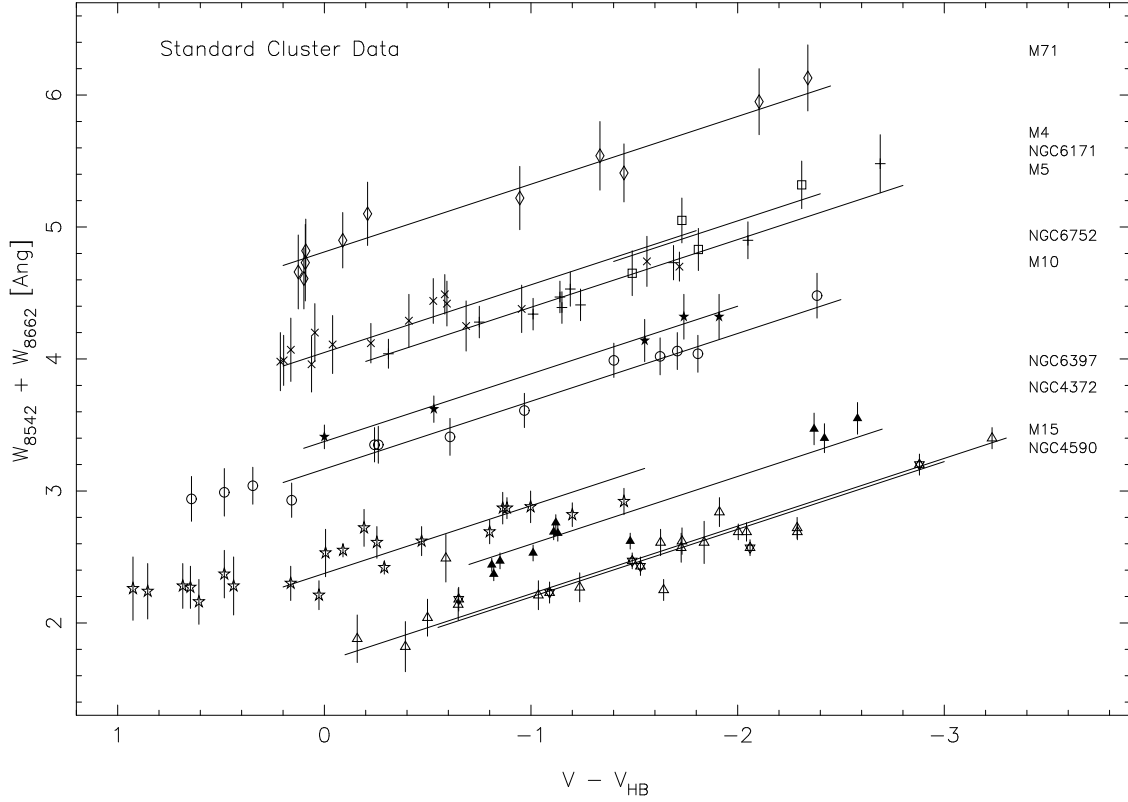


Fig. 2.— Plot of Ca II line strength ($W_{8542} + W_{8662}$) against magnitude difference from the horizontal branch ($V - V_{HB}$) for the 10 standard clusters. In order of increasing $W_{8542} + W_{8662}$ values at $V - V_{HB} = -1.5$, the solid lines are for clusters NGC 4590 (individual stars plotted as open 6-pt star symbols), M15 (open triangles), NGC 4372 (filled triangles), NGC 6397 (open 5-pt stars), M10 (open circles), NGC 6752 (filled 5-pt stars), M5 (plus symbols), NGC 6171 (open squares), M4 (x-symbols), and M71 (open diamonds). The data for each cluster has been fit with a line of slope $-0.51\text{\AA}/\text{mag}$ for $V - V_{HB} \leq 0.2$. Vertical bars on each point show the measurement uncertainty in the line strengths.

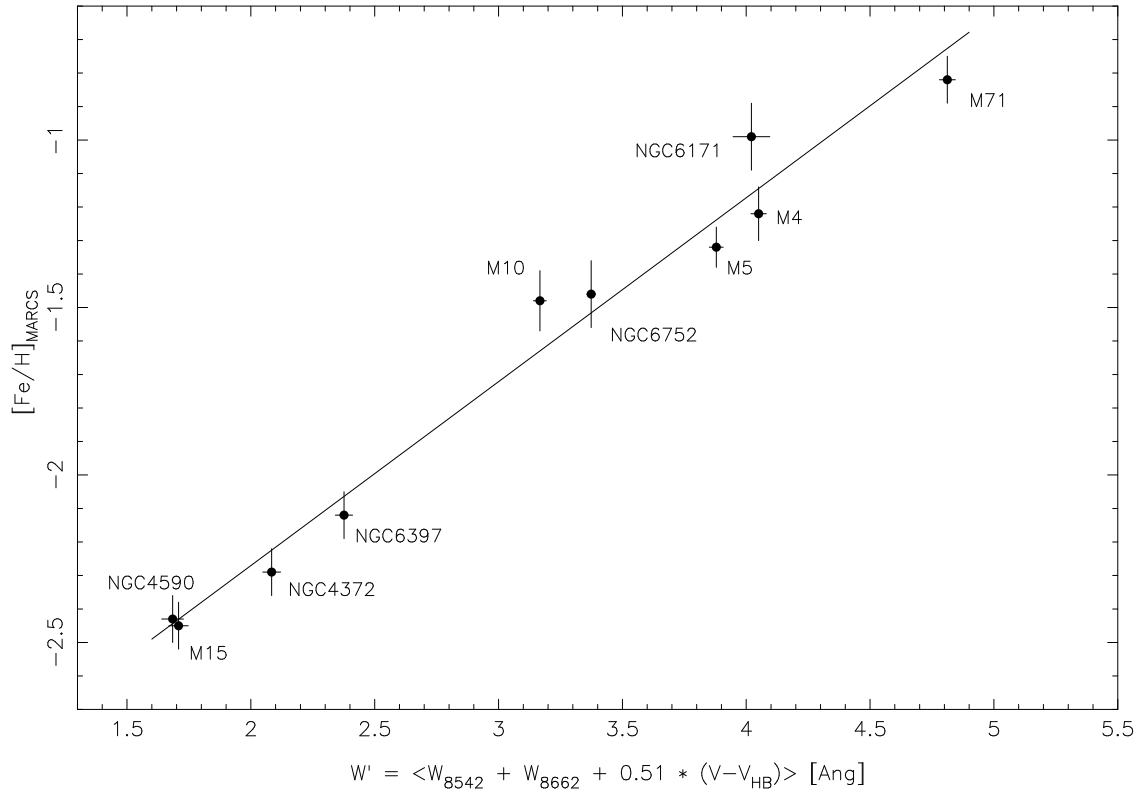


Fig. 3.— Plot of the reduced equivalent width W' for the 10 standard clusters against $[\text{Fe}/\text{H}]$ values from Kraft & Ivans (2003) derived using MARCS model atmospheres. The fitted line has a slope of $0.549 \text{ dex}/\text{\AA}$.

the values of W_{8542} , W_{8662} and their sum, together with their associated uncertainties.

3.2. M22

For the 55 stars in the M22 field with reduced spectra, 51 have velocities compatible with cluster membership. The mean velocity of these stars is $-150 \pm 2 \text{ km s}^{-1}$ which agrees well with the value $-148.9 \pm 0.4 \text{ km s}^{-1}$ tabulated by Harris (1996). The velocities of the other 4 stars clearly exclude them as members. The $W_{8542} + W_{8662}$ values for the member stars were then determined in the same way as for the standard cluster stars. A plot of the values against $V - V_{HB}$ is shown in Fig. 4. Shown also on the Figure is the best fit of a line with a slope of -0.51 \AA/mag ; as for the standard clusters only the 41 M22 members with $V - V_{HB} \leq 0.2$ were included in the fit. For completeness we note that a least squares fit to these 41 points yields a slope of $-0.49 \pm 0.06 \text{ \AA/mag}$ fully consistent with the slope derived from the standard cluster observations.

The average W' value for the 41 M22 stars with $V - V_{HB} \leq 0.2$ is 2.912 ± 0.044 (std error of the mean), which corresponds to an abundance $[\text{Fe}/\text{H}]_{\text{MARCS}} = -1.77$ dex using the calibration given in equation (1) above. The formal uncertainty in this value is small ($0.549 \times 0.044 = 0.02$ dex), but in practice the actual uncertainty will be of order of the calibration uncertainty, i.e. approximately 0.1 dex. Comparison of this value with other determinations is not straightforward. Rutledge et al. (1997a) did not observe M22 and so there is no value for this cluster given in Kraft & Ivans (2003). Carretta & Gratton (1997) give $[\text{Fe}/\text{H}] = -1.48 \pm 0.06$ on their scale but Kraft & Ivans (2003) note that using MARCS models, they derive abundances that are systematically lower by about 0.2 dex than those of Carretta & Gratton (1997) for the same clusters. Zinn & West (1984) give $[\text{Fe}/\text{H}] = -1.75 \pm 0.08$, which is in close accord with our determination. This is not surprising since Kraft & Ivans (2003) note that at metallicities of this order, the difference between their MARCS model abundances (whose scale we have adopted here) and those of Zinn & West (1984) are small. Ivans et al. (2004) uses an abundance of $[\text{Fe}/\text{H}] = -1.7$ dex, presumably on the MARCS scale, while Harris (1996) lists $[\text{Fe}/\text{H}] = -1.64$ for M22. These are again consistent with our determination. Similarly Marino et al. (2009) give a mean metallicity for M22 of $[\text{Fe}/\text{H}] = -1.76 \pm 0.02$ (internal errors only, weighted mean of the UVES and GIRAFFE data), essentially identical to our determination.

We give in Table 2 the ID numbers and positions for the 51 M22 member stars, along with the measured heliocentric radial velocities in km s^{-1} , the magnitude difference from the horizontal branch, ΔV , the individual W_{8542} and W_{8662} measurements in \AA and their errors, as well as their sum, ΣW , and its uncertainty.

Table 1. Standard Cluster Data

ID	RA (2000)	Dec (2000)	Rad Vel (km s ⁻¹)	ΔV (mag)	W_{8542} (\AA)	ϵ	W_{8662} (\AA)	ϵ	ΣW (\AA)	ϵ
M4 1_286	16 23 43.2	-26 31 54	87	-0.53	2.57	0.15	1.87	0.09	4.44	0.17
M4 1_1227	16 23 41.0	-26 31 30	69	-0.58	2.55	0.12	1.94	0.09	4.49	0.15
M4 1_1604	16 23 54.8	-26 31 20	53	-0.23	2.31	0.12	1.81	0.09	4.12	0.15
M4 1_3266	16 23 38.6	-26 30 38	58	-0.41	2.52	0.17	1.77	0.11	4.29	0.20
M4 1_4341	16 23 41.0	-26 30 09	81	0.21	2.41	0.19	1.57	0.11	3.98	0.22

Note. — This table is available in its entirety in a machine-readable form in the online journal. A portion is shown here for guidance regarding its form and content.

Table 2. M22 Member Data

ID	RA (2000)	Dec (2000)	Rad Vel (km s ⁻¹)	ΔV (mag)	W_{8542} (\AA)	ϵ	W_{8662} (\AA)	ϵ	ΣW (\AA)	ϵ
1_232	18 36 41.5	-23 54 39	-148	-0.10	1.68	0.06	1.47	0.06	3.15	0.08
1_756	18 36 41.1	-23 54 33	-136	0.98	1.46	0.15	0.97	0.11	2.43	0.19
1_1211	18 36 42.3	-23 54 28	-144	0.52	1.73	0.11	1.30	0.07	3.03	0.13
1_2276	18 36 37.4	-23 54 17	-146	-0.42	1.61	0.07	1.32	0.05	2.93	0.09
1_3666	18 36 36.3	-23 54 02	-148	-1.57	2.00	0.09	1.55	0.05	3.55	0.10

Note. — This table is available in its entirety in a machine-readable form in the online journal. A portion is shown here for guidance regarding its form and content.

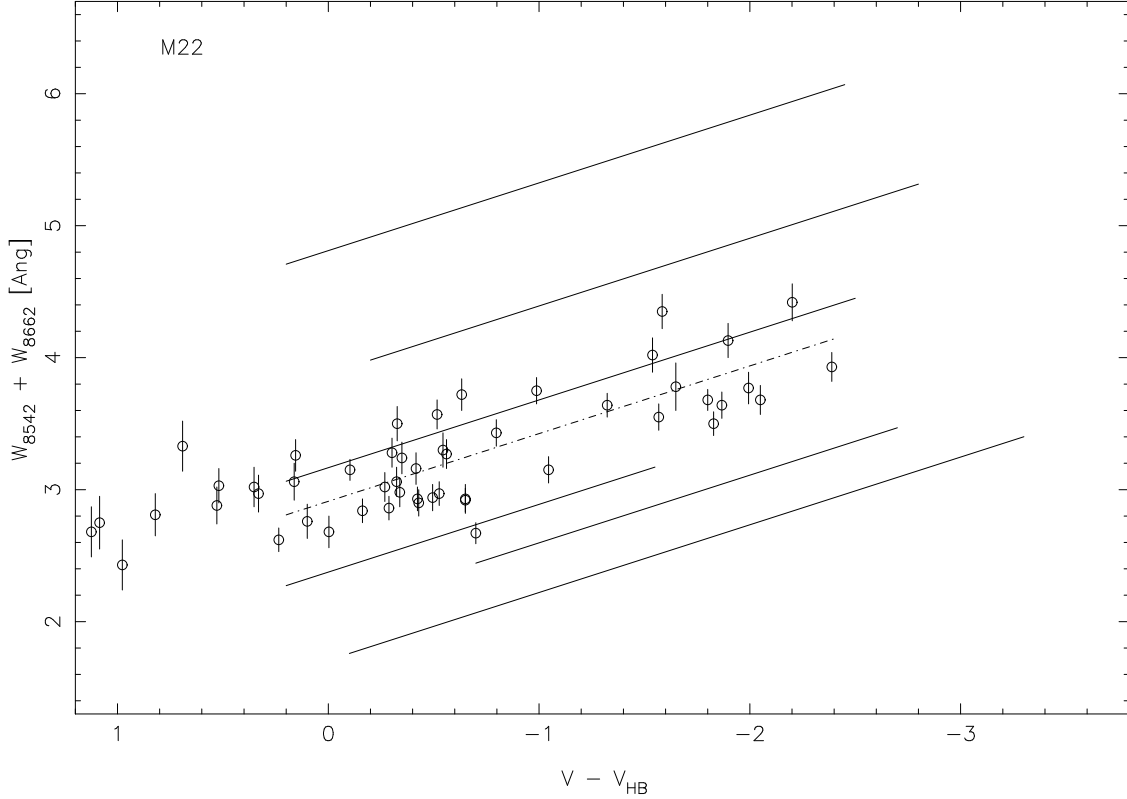


Fig. 4.— Plot of Ca II line strength ($W_{8542} + W_{8662}$) against magnitude difference from the horizontal branch ($V - V_{HB}$) for the 51 M22 members. The solid lines, in order of increasing $W_{8542} + W_{8662}$ values at $V - V_{HB} = -1.5$, are the relations for the standard clusters M15 ($[Fe/H]_{MARC5} = -2.45$), NGC 4372 (-2.29), NGC 6397 (-2.12), M10 (-1.48), M5 (-1.32) and M71 (-0.82). The dot-dash line is the fit of a line of slope $-0.51\text{\AA}/\text{mag}$ to the M22 stars with $V - V_{HB} \leq 0.2$. Vertical bars on each point show the measurement uncertainty in the line strength.

4. Discussion

The most striking thing about the distribution of points in Fig. 4 is the large apparent scatter about the fitted line: the rms dispersion in $W_{8542} + W_{8662}$ at fixed $V - V_{HB}$ for the 41 stars with $V - V_{HB} \leq 0.2$ is 0.28 \AA , which is considerably larger than the mean measurement error, 0.11 \AA . This stands in stark contrast to the situation for the standard clusters. For example, the stars observed in the standard clusters M15, NGC 6397 and M10 have mean measurement errors of 0.11, 0.11 and 0.14 \AA , respectively, values comparable to that for M22. Yet for these clusters the rms dispersions about the fitted line are 0.16, 0.13, and 0.08 \AA , comparable to errors and substantially less than is the case for M22. It is also clear from Fig. 4 that the fainter stars in M22 show a similar dispersion. We now investigate possible origins for this large spread.

The first possibility is that the sample is contaminated with non-members. This seems very unlikely: the observed velocity dispersion of the stars classified as members is 12 km s^{-1} , which is similar to the observed dispersion for other member sets. For example, the velocity dispersions of the member stars in the standard clusters M15, NGC 6397 and M10 are 20, 12 and 8 km s^{-1} , respectively. Further, the M22 stars whose measured velocities lie furthest from the mean are not distinguished from the remainder of the sample in Fig. 4, nor do the stars that stand furthest from the mean line in the figure have velocities that are notably discrepant. We conclude that all the stars in Fig. 4 are indeed likely members of M22.

The second possibility is that the large scatter is produced by differential reddening across the observed field. Such reddening variations would induce scatter in the $V - V_{HB}$ values and thus potentially increase the scatter about the mean line. To investigate this possibility we first examined the spatial location of the observed stars. Specifically, we have split the sample into two groups, those that lie above the mean line (potentially more reddened on average, 19 stars) and those that lie below the mean line (potentially less reddened, 22 stars). Figure 5 shows the outcome: the first group are plotted as red stars while the second group are plotted as blue squares. There is clearly no straightforward segregation of the red and blue points in the Figure. Consequently, if reddening variations are the explanation, then the variations must occur on small scales of order $\sim 20\text{--}30''$, perhaps less.

While it is unclear whether reddening variations on such scales are present in our M22 field, we note that Lyons et al. (1995) have shown that $E(B - V)$ variations of order 0.05 mag can occur on scales as small as few arcsecs in the field of the globular cluster M4. Thus we need to at least enquire into the size of the reddening variations required to produce the scatter in Fig. 4. We have done this via Monte-Carlo simulations. We start with the assumption that there is no intrinsic line strength spread other than that induced by the measurement errors in the $W_{8542} + W_{8662}$ values. The trials are conducted as follows: for each of the 41 $V - V_{HB}$ values with $V - V_{HB} \leq 0.2$, the mean line in Fig. 4 is used to generate initial $W_{8542} + W_{8662}$ values. These initial values are then altered by random draws from a gaussian distribution with mean zero and standard deviation equal to mean error in the observed $W_{8542} + W_{8662}$ values, which is 0.11 \AA . In the absence of any

additional broadening mechanism, the average over many trials would have a dispersion about a fitted line of slope $-0.51 \text{ \AA}/\text{pix}$ equal to the mean observational errors, and a W' value equal to the observed value. We verified that this is indeed the case. To simulate the effects of differential reddening we then perturbed the $V - V_{HB}$ values with random draws again from a gaussian, keeping the $W_{8542} + W_{8662}$ values (after perturbation with the error distribution) unaltered. This second gaussian has mean zero and a standard deviation as input, representing $\sigma(E(B - V))$. After the $V - V_{HB}$ values are perturbed, assuming $A_V = 3.2 E(B - V)$, a line of slope $-0.51 \text{ \AA}/\text{pix}$ is fit taking care to exclude any stars whose perturbed $V - V_{HB}$ value exceeds 0.2, and the corresponding W' and dispersion about the line calculated. We find that in order to consistently reproduce the observed dispersion of 0.28 \AA with mean measurement errors of 0.11 \AA , we require $\sigma(E(B - V)) \approx 0.12\text{--}0.15 \text{ mag}$. Clearly adopting a larger value than 3.2 for $R = A_V/E(B - V)$ would increase the dispersion about the mean line for a given $\sigma(E(B - V))$. However, we find that even adopting $R = 3.6$ (cf. Appendix F of Bessell et al. 1998), the result is not materially altered — the minimum $\sigma(E(B - V))$ required for the observed dispersion to be consistently realized in the trials becomes 0.11 rather than 0.12 mag.

These values of $\sigma(E(B - V))$ are considerably larger than existing estimates of the degree of differential reddening in the field of M22. For example, Monaco et al. (2004) estimate a maximum *range* in $E(B - V)$ across the entire face of the cluster as 0.06 mag, larger variations would be inconsistent with their data. We conclude therefore that there is an intrinsic spread in the $W_{8542} + W_{8662}$ values for M22, over and above that due to any differential reddening.

4.1. The Abundance Spread in M22

If the intrinsic spread in the $W_{8542} + W_{8662}$ values for the M22 stars is not due to non-member contamination and is not primarily the result of differential reddening, then the remaining alternative is that it is the consequence of an intrinsic abundance spread in the cluster. Noting that for each individual star we can define a W' value as $W_{8542} + W_{8662} + 0.51(V - V_{HB})$, equation (1) can then provide an abundance estimate $[\text{Fe}/\text{H}]_{\text{MARCS}}$ for each individual star. We show in Fig. 6 a generalized histogram made from the individual $[\text{Fe}/\text{H}]_{\text{MARCS}}$ values and the corresponding abundance uncertainties that follow from the measurement uncertainties in the $W_{8542} + W_{8662}$ values. These have a mean value of 0.06 dex. We also show in the figure the contributions to the total from the stars below (more metal-poor) and above (more metal-rich) the fitted line in Fig. 4, which corresponds to an abundance $[\text{Fe}/\text{H}] = -1.77 \text{ dex}$. The method assumes that there is no significant contribution to the abundance determinations from differential reddening. This is likely to be the case for the following reason. If the differential reddening has a range $\Delta E(B - V) \sim 0.06 - 0.08 \text{ mag}$ (e.g., Monaco et al. 2004; Anthony-Twarog et al. 1995), then presumably $\sigma(E(B - V)) \sim 0.02$ and thus $\sigma(A_V) \sim 0.06 \text{ mag}$ with the same value for $\sigma(V - V_{HB})$. This converts to $\sigma([\text{Fe}/\text{H}]) \sim 0.02 \text{ dex}$, which is much smaller than the observed value of $\sigma([\text{Fe}/\text{H}]) = 0.15 \text{ dex}$. This contrasts with the photometric case where $\sigma(V - I)$ from differential reddening of size $\sigma(E(B - V)) \approx 0.02$

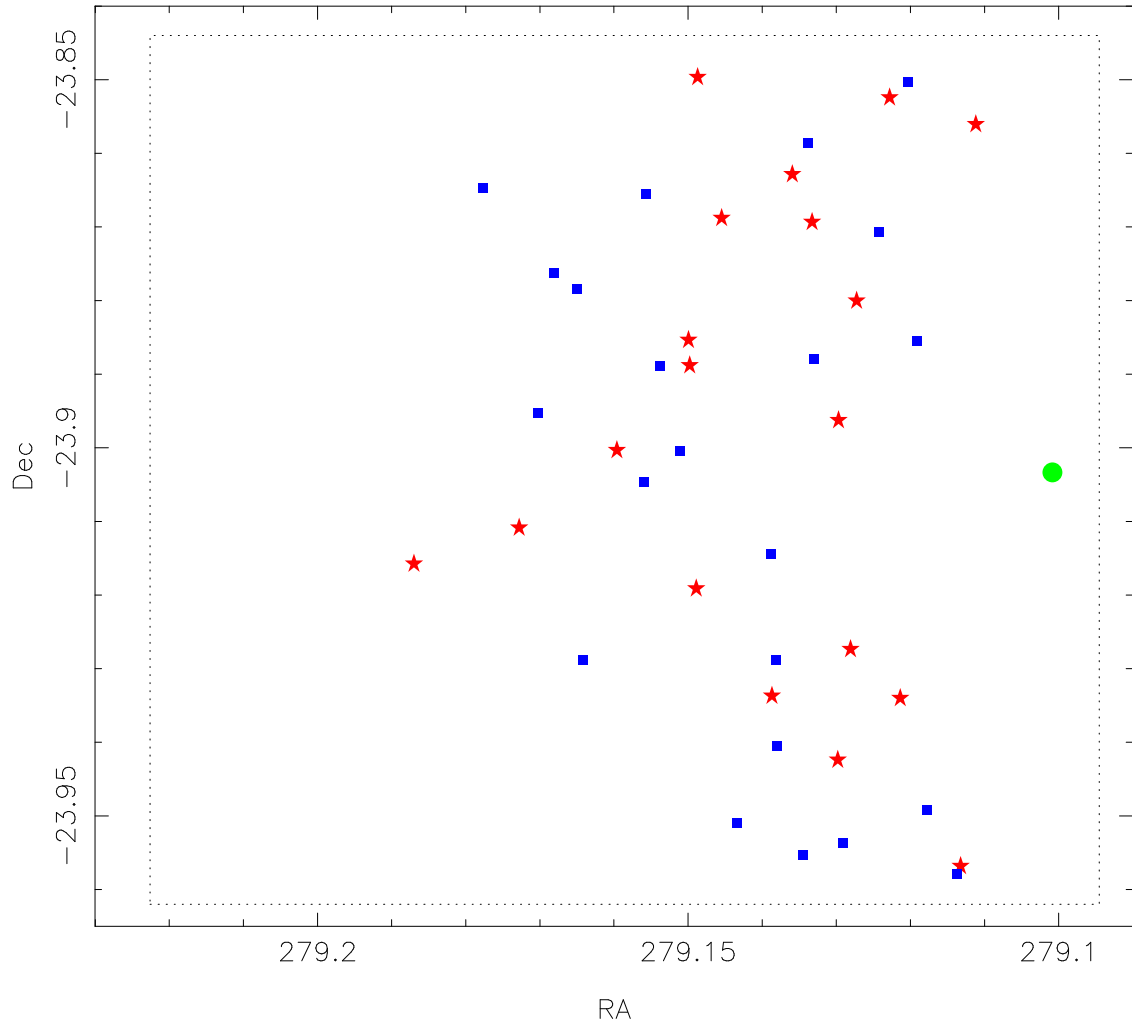


Fig. 5.— Plot of the positions of the 19 M22 member stars that lie above the mean relation in Fig. 4 (red stars) and of the 22 stars that lie below the relation (blue squares). The $6.8' \times 6.8'$ field-of-view from which the observed stars were selected is outlined by the dotted lines. The cluster center is shown by the green circle. Note that there is no obvious spatial separation of the red and blue symbols.

mag, and $\sigma(V - I)$ from $\sigma([\text{Fe}/\text{H}])_{int} \approx 0.15$ dex are comparable in size and thus more difficult to distinguish.

Figure 6 clearly shows that there are multiple components to the abundance distribution in M22 — it rises rapidly to a narrow peak at $[\text{Fe}/\text{H}]_{MARC\text{S}} = -1.88$ yet there is a broader tail towards higher abundances. We can quantify this distribution in a number of ways. For example, for the 22 stars in metal-poor group, the inter-quartile range is only 0.05 dex, while for the 19 stars in the metal-rich group, the inter-quartile range is notably larger, 0.15 dex. The median abundance for this group is $[\text{Fe}/\text{H}]_{MARC\text{S}} = -1.64$ and the most metal-rich star has $[\text{Fe}/\text{H}]_{MARC\text{S}} = -1.43 \pm 0.07$. The most metal-poor star has $[\text{Fe}/\text{H}]_{MARC\text{S}} = -2.1 \pm 0.05$ and it is 0.14 ± 0.07 dex more metal-poor than the next most metal-poor star. Whether this star represents a separate third metallicity grouping at low abundances and with a small fraction of the total (few percent at most), or is simply a statistical outlier, cannot be determined without a larger sample of member stars. For the entire sample the inter-quartile range is 0.24 dex, which is comparable to the M22 abundance ranges found by the earlier spectroscopic studies of Norris & Freeman (1983) and Lehnert et al. (1991), though it is clearly in conflict with the results of Ivans et al. (2004). Our results are summarised in Table 3. We defer to the next section a comparison with the results of Marino et al. (2009).

We can also take ‘toy’ models for the intrinsic abundance distribution and compare them with the observed distribution after convolution with the measurement errors. One such model is shown in the upper panel of Fig. 7. Here we have assumed that the M22 stars consist of two populations: one with abundances uniformly distributed between $[\text{Fe}/\text{H}] = -1.95$ and -1.83 making up 44% of the total, and a second with abundances uniformly distributed between -1.83 and -1.50 dex and 56% of the total. This abundance distribution is shown in the insert in the upper panel of the figure. Convolution with the measurement errors then gives the dot-dash line, which is an acceptable representation of the observed data. The contributions of the two components are shown by the dotted lines. We have not conducted an exhaustive parameter search so it is likely that other intrinsic abundance distributions could produce similar fits to the observations, *although two components with different abundance ranges does seem to be a requirement*. We note that the

Table 3. M22 Abundance Data

Sample	N	$\langle[\text{Fe}/\text{H}]\rangle$	$\sigma_{obs}([\text{Fe}/\text{H}])$	IQR
All	41	-1.77	0.15	0.24
Metal-Rich Group ^a	19	-1.63	0.09	0.15
Metal-Poor Group ^b	22	-1.89	0.07	0.05

^aStars with $[\text{Fe}/\text{H}] > -1.77$

^bStars with $[\text{Fe}/\text{H}] < -1.77$

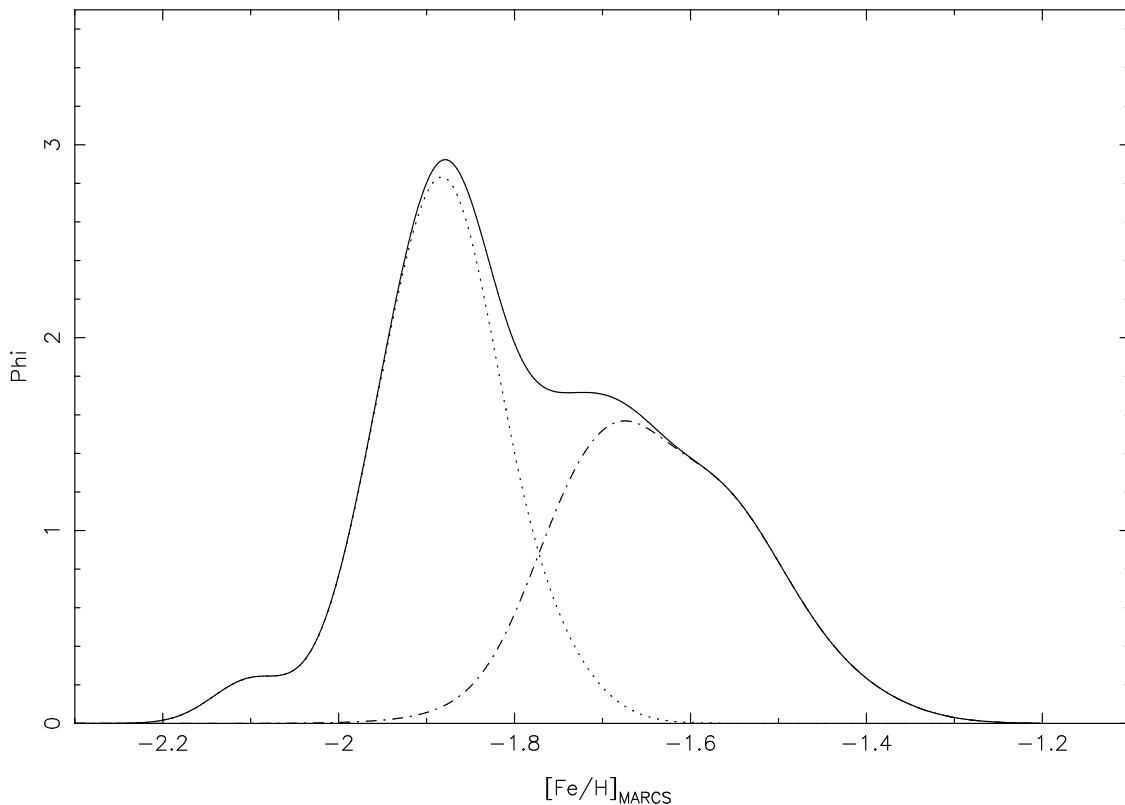


Fig. 6.— A generalized histogram (solid line) of the individual $[\text{Fe}/\text{H}]_{\text{MARCS}}$ values for the 41 M22 stars with $V - V_{HB} \leq 0.2$. Each value has the abundance uncertainty from the uncertainty in the $W_{8542} + W_{8662}$ measurement. Shown also are the generalized histograms for the 22 stars below the fitted line in Fig. 4 (dotted line), and for the 19 stars above the fitted line (dot-dash line).

model does not reproduce the extreme metal-poor tail of the observed distribution adequately. A third component could no doubt be added to the model to fix this, but given that the metal-poor extension results from a single star, the addition of a third component does not seem warranted at this stage. As noted above, a larger sample of member stars is needed to fully characterize the most metal-poor part of the distribution. We note also that assuming a single abundance for the metal-poor group does not fit the observations adequately — a range in abundance in this population is apparently required. However, we have not included the effects of differential reddening, which, as outlined above, could induce $\sigma([\text{Fe}/\text{H}]) \sim 0.02$ dex. Consequently, the extent of the metallicity range in the metal-poor group might well be smaller than assumed in this toy model.

We can also compare the observed abundance distribution with the predictions of simple models of chemical evolution. One of the simplest such model is that in which star formation proceeds in gas whose initial abundance is Z_0 under the assumption of instantaneous recycling and with the rate of gas loss from the system proportional to the star formation rate. In such a model the metallicity distribution function $f(Z)$ is characterized solely by Z_0 and by the mean abundance $\langle Z \rangle$ (e.g., Hartwick 1976; Norris et al. 1996). In the lower panel of Fig. 7 we show a comparison of the prediction of such a model with the M22 observations. The model has been calculated with $\log(Z_0/Z_{sun}) = -1.95$ and $\log(\langle Z \rangle/Z_{sun}) = -1.77$ dex, which is the observed sample mean abundance. We assume $Z_{sun} = 0.017$. The model distribution was then convolved with the 0.06 dex mean $[\text{Fe}/\text{H}]$ error. The fit to the observations is adequate, but it does seem likely that to improve the fit, a second component with higher values for Z_0 and $\langle Z \rangle$ would be required (cf. Norris et al. 1996). However, it is not clear what additional insight would result from computing such a two component model given that it does not help understand how such a model might arise physically.

Additional insight can be gained by comparing the M22 abundance distribution with that for ω Cen (e.g., Norris et al. 1996). To do this we have taken the $[\text{Ca}/\text{H}]$ abundances for ~ 500 ω Cen red giants from Norris et al. (1996) and generated a generalized histogram using the average abundance error given by Norris et al. (1996), which, at 0.05 dex, is very similar to that for the M22 observations. The ω Cen histogram was then shifted first by -0.4 dex, which corresponds to the mean $[\text{Ca}/\text{Fe}]$ ratio for ω Cen red giants (e.g., Norris & Da Costa 1995b), and then by a further -0.09 dex to match the $[\text{Fe}/\text{H}]$ of the peak of the M22 abundance distribution. It was then scaled so that the peak height coincided with that for M22. The outcome is shown in Fig. 8. The two distributions are not significantly different on the metal-poor side of the peak given the smaller M22 sample. It is clear, however, that the ω Cen distribution is broader on the metal-rich side, though the ‘rate of decline’ away from the peak is similar. It also appears that the ‘second abundance peak’ in M22 is closer in abundance to the main peak than is the case for ω Cen. Furthermore, the ω Cen abundance distribution continues to significantly higher abundances than M22, a result that is not obviously an outcome of the smaller size of the M22 observed sample. Despite these differences, the general similarity between the two distributions suggests that they could readily be the result of the same physical process or processes, except that it has gone on longer in ω Cen, or

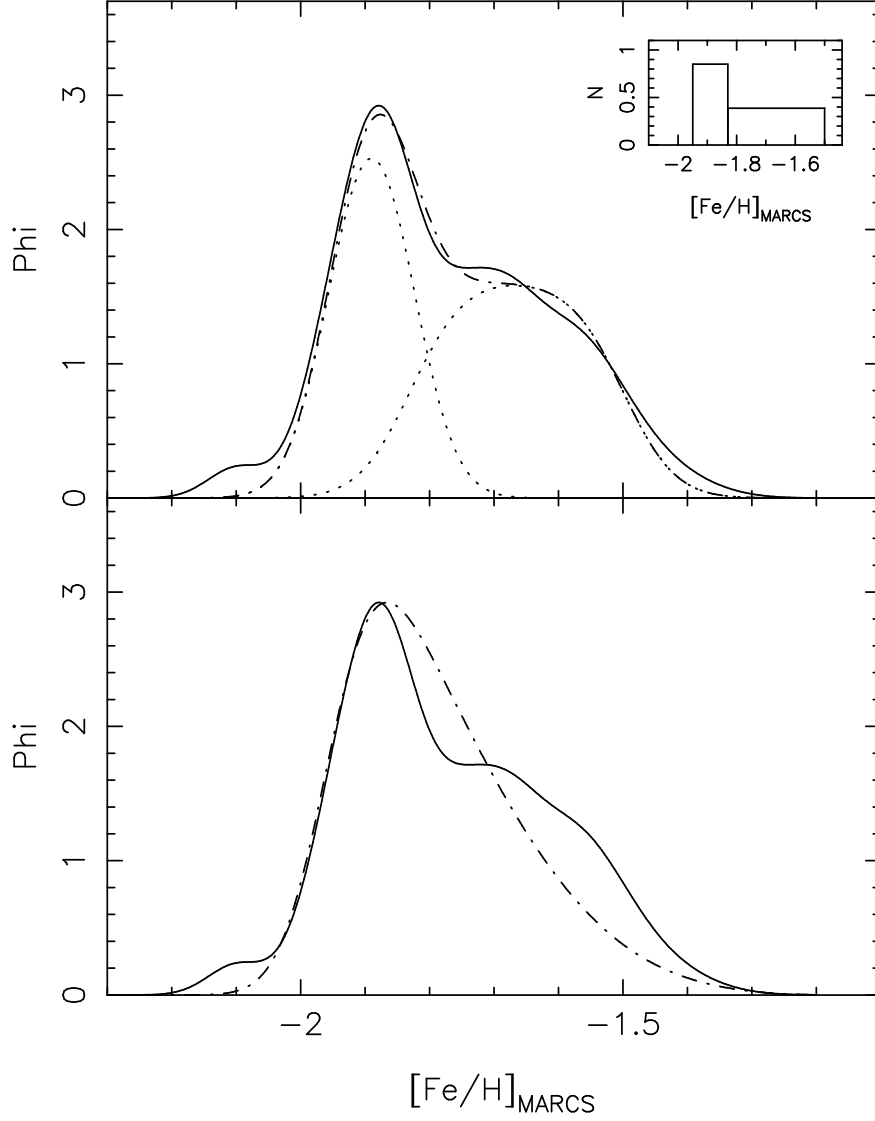


Fig. 7.— (a) *Upper panel.* The solid line is the generalized histogram of the individual M22 $[\text{Fe}/\text{H}]_{\text{MARCS}}$ abundances from Fig. 6. The dot-dash line, which is a reasonable representation of the observations, is the result of convolving the abundance distribution shown in the insert with the measurement errors. This distribution has two components, one with abundances distributed uniformly between $[\text{Fe}/\text{H}]_{\text{MARCS}} = -1.95$ and -1.83 , and the other distributed uniformly between -1.83 and -1.50 dex. The population ratio is 1 to 1.25. The contributions of each component are shown as dotted lines. (b) *Lower panel.* The solid line is again the generalized histogram of the individual M22 $[\text{Fe}/\text{H}]_{\text{MARCS}}$ abundances from Fig. 6. The dot-dash line is the abundance distribution for a simple chemical model in which the rate of gas loss is proportional to the star formation rate. The model assumes an initial abundance of $\log(Z_0/Z_{\text{sun}}) = -1.95$ and has $\log(\langle Z \rangle/Z_{\text{sun}}) = -1.77$ dex corresponding to the mean abundance of the observed sample.

terminated sooner in M22, perhaps because of the difference in mass between the systems.

Given that, in contrast to M22, most globular clusters are homogeneous with respect to heavy element abundances, the similarity between the M22 and ω Cen abundance distributions seen in Fig. 8 naturally leads to the following speculation. The unusual properties of ω Cen have frequently led to the interpretation that the stellar system is the nuclear remnant of a now disrupted dwarf galaxy (e.g., Freeman 1993). Consequently, it is plausible to suggest that M22 may also be a nuclear remnant of a disrupted dwarf galaxy. The fact that M54, the central star cluster of the Sgr dwarf, also shows an internal abundance range lends further support to the suggestion. The stellar system ω Cen lies in a tightly bound retrograde orbit which never rises very far above the Galactic Plane (e.g., Dinescu et al. 1999). Yet Bekki & Freeman (2003) have shown that no inconsistencies arise in evolving a nucleated dwarf galaxy in the tidal gravitational field of the Galaxy from an initial large galactocentric distance to a nuclear remnant with an orbit resembling that of the present-day ω Cen. As regards M22, the compilation of Dinescu et al. (1999) shows that its orbit is fairly typical for inner halo objects (cf. Carollo et al. 2007). It is strongly prograde ($\Theta = 178 \pm 20 \text{ km s}^{-1}$) with apo- and pericentric distances of approximately 9.5 and 2.9 kpc, respectively, and a maximum height above the plane of 1.8 kpc (Dinescu et al. 1999). Given the results of Bekki & Freeman (2003) for ω Cen, it seems likely that one could also start with a nucleated dwarf galaxy at large galactocentric distances and evolve it such that the nuclear remnant has an orbit similar to that of M22.

It is also noteworthy that both ω Cen and M22 have strong blue horizontal branch populations, as does M54. In the case of M22 this is not unusual given its relatively low mean metal abundance and relatively small distance from the Galactic Center: in the terminology of Zinn (1993) and Lee et al. (1994) M22 is an ‘old-halo’ cluster. But it is also interesting to note that M22, ω Cen and M54, the three clusters for which there is definite evidence for the presence of internal abundance ranges, are all in the ‘EHB’ classification of Lee et al. (2007). Lee et al. (2007) have shown that the EHB clusters form a kinematically distinct group, and argue that such clusters have their origin as the cores or central star clusters of stellar systems accreted during the earliest phases of the formation of the Galaxy. This is then consistent with our interpretation of M22 and its unusual properties.

4.2. Comparison with the results of Marino et al. (2009)

In a recent paper Marino et al. (2009) have analyzed high dispersion UVES spectra for 17 red giants in M22, supplemented by lower resolution GIRAFFE spectra for a further 14 stars (one of which is in common with the UVES set). The results can be summarized as follows. The distribution of the abundances of the *s*-process elements Y, Zr and Ba in the UVES sample is apparently bimodal, with one group of stars showing significantly larger average values of $[(Y, \text{Zr and Ba})/\text{Fe}]$ compared to the other. Specifically, in the UVES sample, 7 of the 17 stars ($\sim 40\%$) have $\langle [s/\text{Fe}] \rangle = 0.46 \pm 0.03$ while the remainder have $\langle [s/\text{Fe}] \rangle = 0.02 \pm 0.02$ dex (errors are internal

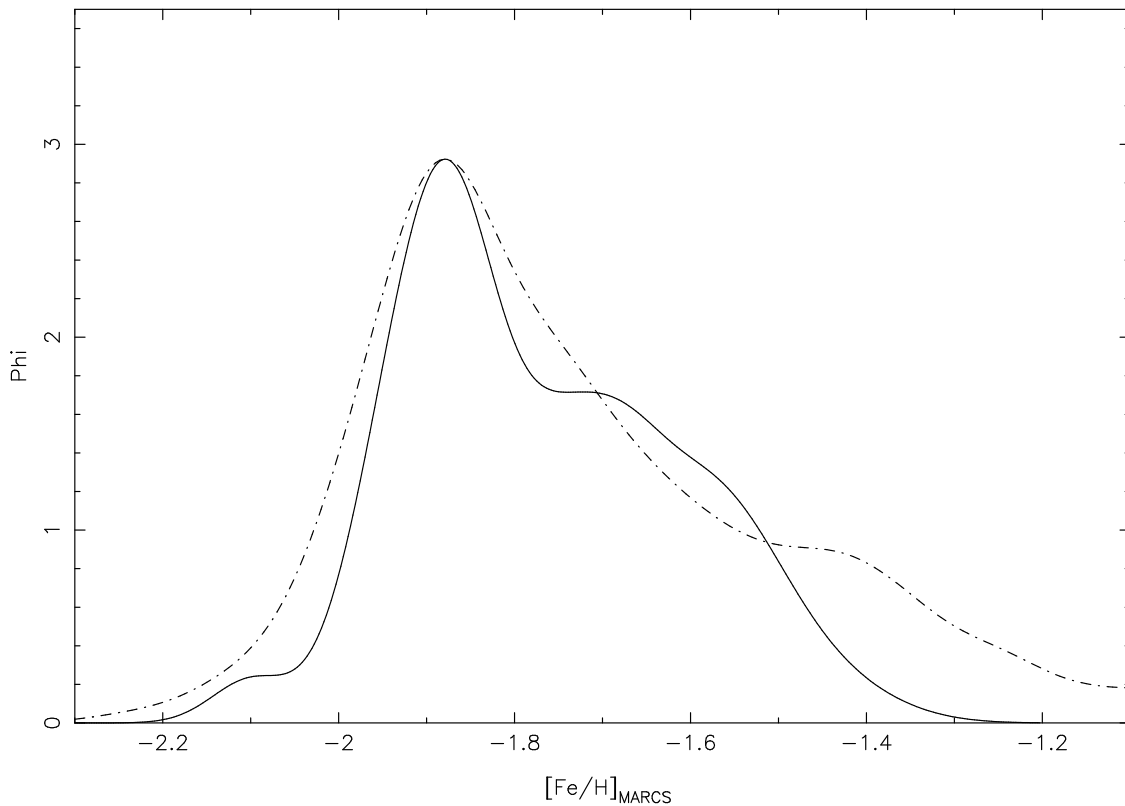


Fig. 8.— The solid line is the generalized histogram of the individual M22 $[\text{Fe}/\text{H}]_{\text{MARCS}}$ abundances from Fig. 6. The dot-dash line is the abundance distribution generalised histogram for ω Cen from Norris et al. (1996). It has been shifted horizontally and scaled vertically to the peak of the M22 distribution.

only). The [Ba/Fe] values for the stars observed with GIRAFFE are consistent with this result. Moreover, for the UVES sample, the *s*-process rich group has both higher average [Fe/H] and [Ca/H] abundances, by 0.14 ± 0.03 dex and 0.25 ± 0.04 dex, respectively. For the GIRAFFE sample the difference in the average [Fe/H] values is 0.18 ± 0.04 dex. The interquartile range in [Fe/H] for the full sample is 0.16 dex, with the most metal-poor star at [Fe/H] = -1.94 and the most metal-rich at [Fe/H] = -1.59 , with (internal) uncertainties of 0.09 dex. These values are reminiscent of the earlier work of Norris & Freeman (1983) and Lehnert et al. (1991), and are entirely consistent with the results presented here.

There are 3 stars in common between the Marino et al. (2009) UVES observations and the sample presented here, with Marino et al. (2009) stars 200068, 200101 and 200083 corresponding to our stars 1_16051, 1_3683 and 1_10101. For these stars, which have [Fe/H] values of -1.84 , -1.74 and -1.63 in Marino et al. (2009), the differences in [Fe/H] values in the sense of Marino et al. (2009) abundance minus that derived here, are 0.09 ± 0.11 , 0.02 ± 0.13 and 0.01 ± 0.11 dex, where the error given is the combined internal uncertainty. Clearly, although the sample is small, there is no evidence for any systematic offset (the mean difference is 0.04 dex) and the standard deviation of the differences, ± 0.05 dex, is consistent with the errors. Consequently, we have used a (two-sided) K-S test to compare the [Fe/H] distribution for the 30 stars in the Marino et al. (2009) full sample with that for the 41 stars with [Fe/H] values measured here. We find that the null hypothesis, namely that the two samples come from the same underlying distribution, cannot be ruled out, even at a 10% significance level. This has one immediate consequence. As noted in the Introduction, Piotto (2009) has shown that in a *HST*-based c-m diagram the M22 sub-giant branch has a bimodal structure with the upper (brighter) branch contributing $38 \pm 5\%$ and the lower $62 \pm 5\%$ of the total (see Marino et al. 2009). One interpretation of this bimodal structure in the c-m diagram is that it reflects the abundance distribution in the cluster, with the fainter sub-giant branch corresponding to the more metal-rich population, with a negligible age difference. Marino et al. (2009) note, however, that for a difference in average [Fe/H] of 0.14 dex, the predicted difference in the sub-giant branch location is ~ 0.10 mag in *F606W*, smaller than the observed difference of ~ 0.17 mag. Further, in Marino et al. (2009), the metal-rich group is less than half the sample ($37 \pm 13\%$), in contrast to the situation in the c-m diagram. Our data alleviate both of these concerns. For example, the difference in average abundance between the two populations shown in the insert in the upper panel of Fig. 7 is 0.23 dex, which would predict a bigger magnitude difference on the sub-giant branch. Also, the ratio of the populations, 56% metal-rich to 44% metal-poor, is more in accord with the observed ratios in the c-m diagram. Detailed modeling of the c-m diagram is required to place limits on the abundance distribution, and variations in other plausible parameters such as total CNO and age, required to reproduce the observations.

One further point can be made concerning M22 and ω Cen. We argued above that the overall M22 abundance distribution is similar to that of ω Cen, except that M22 lacks the tail to higher abundances. The availability of high dispersion abundance analyses for M22 stars from

Marino et al. (2009) means that the comparison can now be extended to individual abundance ratios, using ω Cen red giant results from, for example, Norris & Da Costa (1995b). We show an example in Fig. 9. The upper panel shows $[\text{Ba}/\text{Fe}]$ as a function of $[\text{Fe}/\text{H}]$ for 40 ω Cen red giants from Norris & Da Costa (1995b). The $[\text{Ba}/\text{Fe}]$ ratio rises with increasing $[\text{Fe}/\text{H}]$ until $[\text{Fe}/\text{H}] \approx -1.3$ after which the Ba and Fe abundances change in lock-step. The dot-dash line is a least squares fit to the stars with $[\text{Fe}/\text{H}]$ between -1.9 and -1.3 , excluding the three metal-poor stars with high $[\text{Ba}/\text{Fe}]$, at least one of which is a carbon-star (see Norris & Da Costa 1995b). The lower panel shows the $[\text{Ba}/\text{Fe}]$ ratios for the 30 M22 stars in Marino et al. (2009). The dot-dash line is reproduced from the upper panel except that it has been shifted to lower $[\text{Fe}/\text{H}]$ by 0.2 dex. While there are differences in detail, such as the metal-poor stars in M22 having $[\text{Ba}/\text{Fe}] \approx 0.0$ dex but -0.2 in ω Cen, the relations are clearly similar, indicating that it is likely similar enrichment processes went on in both clusters.

5. Conclusions

We have shown here that there is strong evidence for the existence of a significant internal abundance range in the globular cluster M22, consistent with the results of Marino et al. (2009). The cluster thus joins ω Cen and M54 as the only Galactic globular clusters in which intrinsic $[\text{Fe}/\text{H}]$ ranges have been established. The M22 abundance distribution rises sharply from low abundances to a distinct peak at $[\text{Fe}/\text{H}] \approx -1.9$, with a broad tail to higher abundances. Consequently, it is probable that at least two components are needed to describe the distribution. The abundance distribution also bears a qualitative similarity to that for ω Cen, although the overall scale in M22 is considerably smaller. Nevertheless, the similarity suggests a comparable origin for the abundance ranges in both systems. Indeed, given that M54 is currently the central star cluster of the Sgr dSph, and that ω Cen is frequently postulated as being the remnant nucleus of a disrupted dwarf galaxy, it seems logical to conclude that M22 may also be the remnant nucleus or nuclear star cluster of a disrupted dwarf galaxy.

EVH acknowledges support from the Italian National Project PRIN MIUR 2007 “Galactic astroarchaeology: the local route to Cosmology” (P.I. F. Matteucci). We are also grateful to Anna Marino for providing details from her M22 study and to the referee for comments that improved the presentation.

Facilities: VLT

REFERENCES

- Anthony-Twarog, B. J., Twarog, B. A., & Craig, J. 1995, *PASP*, 107, 32
- Armandroff, T. E., & Da Costa, G. S. 1991, *AJ*, 101, 1329

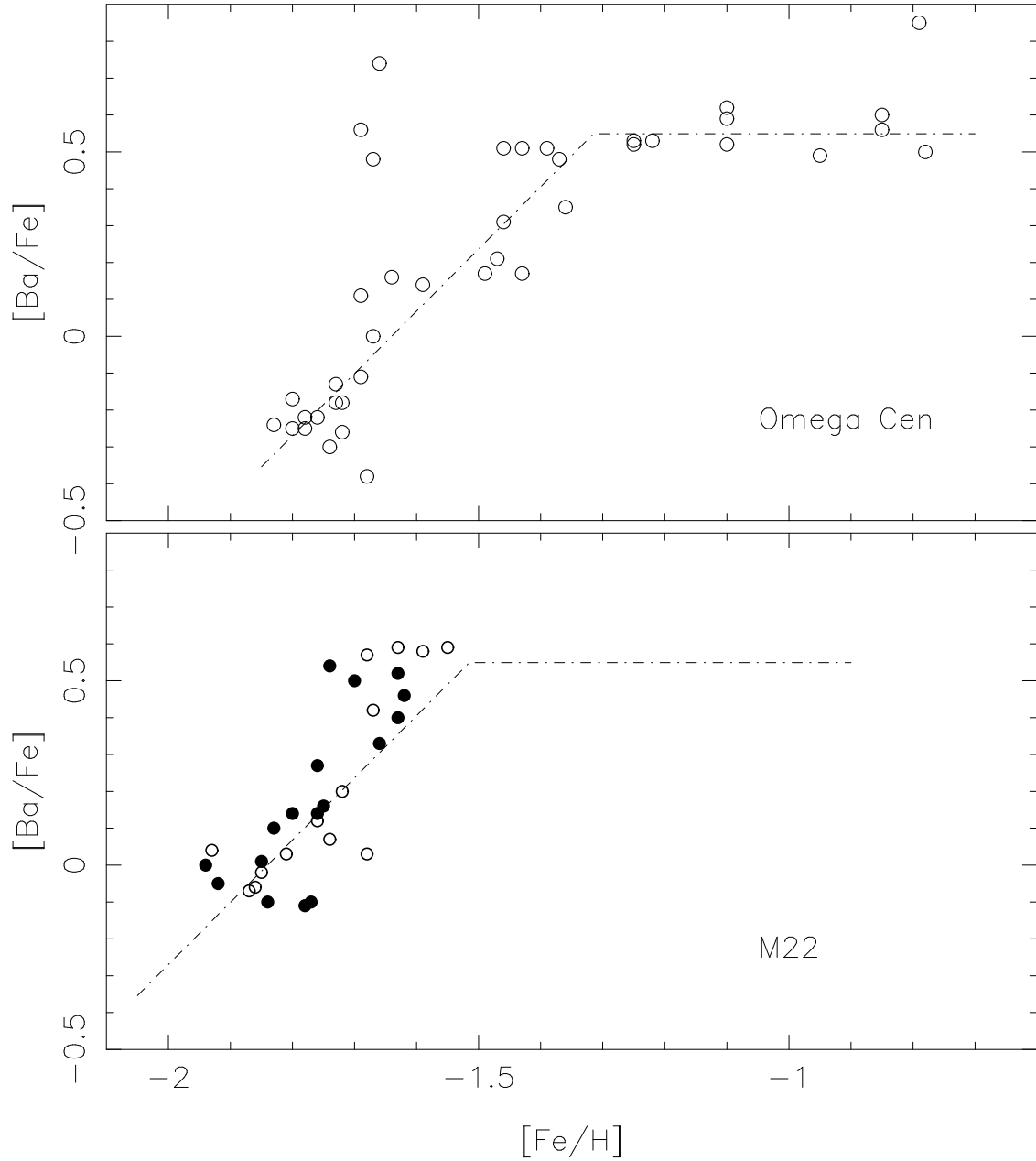


Fig. 9.— $[Ba/Fe]$ as a function of $[Fe/H]$ for red giants in ω Cen using data from Norris & Da Costa (1995b), *upper panel*, and for M22 from Marino et al. (2009), *lower panel*. The dot-dash lines have been fitted to the ω Cen distribution (see text for details) and are reproduced in the lower panel after a shift to lower $[Fe/H]$ values by 0.2 dex. In the lower panel the filled circles are the stars with UVES data, the open circles are the GIRAFFE data. The enrichment processes appear similar in both stellar systems.

- Battaglia, G., Irwin, M., Tolstoy, E., Hill, V., Helmi, A., Letarte, B., & Jablonka, P. 2008, MNRAS, 383, 183
- Bekki, K., & Freeman, K. C. 2003, MNRAS, 36, L11
- Bekki, K., & Norris, J. E. 2006, ApJ, 637, 109
- Bellazzini, M., Ibata, R. A., Chapman, S. C., Mackey, A. D., Monaco, L., Irwin, M. J., Martin, N. F., Lewis, G. F., & Dalessandro, E. 2008, AJ, 136, 1147
- Bessell, M. S., Castelli, F., & Plez, B. 1998, A&A, 333, 231
- Carretta, E. & Gratton, R. 1997, A&AS, 121, 95
- Carollo, D., Beers, T. C., Lee, Y. S., Chiba, M., Norris, J. E., Wilhelm, R., Sivarani, T., Marsteller, B., Munn, J. A., Bailer-Jones, C. A. L., Fiorentin, P. R., & York, D. G. 2007, Nature, 450, 1020
- Da Costa, G. S., & Armandroff, T. E. 1990, AJ, 100, 162
- Da Costa, G. S., & Armandroff, T. E. 1995, AJ, 109, 2533
- Dinescu, D. I., Girard, T. M., & van Altena, W. F. 1999, AJ, 117, 1792
- Freeman, K. C. 1993, The Globular Cluster—Galaxy Connection (ASP Conf. Ser. 48), ed. G. H. Smith & J. P. Brodie (San Francisco, CA: ASP), 608
- Freeman, K. C., & Rodgers, A. W. 1975, ApJ, 201, L71
- Gratton, R., Sneden, C., & Carretta, E. 2004, ARA&A, 42, 385
- Gullieuszik, M., Held, E. V., Saviane, I., & Rizzi, L. 2009, A&A, 500, 735
- Harris, W.E. 1996, AJ, 112, 1487
- Hartwick, F. D. A. 1976, ApJ, 209, 418
- Hesser, J. E., & Harris, G. L. 1979, ApJ, 234, 513
- Hesser, J. E., Hartwick, F. D. A., & McClure, R. D. 1977, ApJS, 33, 471
- Horne, K. 1986, PASP, 98, 609
- Ivans, I. I., Sneden, C., Wallerstein, G., Kraft, R. P., Norris, J. E., Fulbright, J. P., & Gonzalez, G. 2004, Mem. S. A. It., 75, 286
- Izzo, C., & Larsen, J. M., 2008, FORS Pipeline User Manual, VLT-MAN-ESO-19500-4106, Issue 2.0, ESO Garching, 2008-09-09

- Kraft, R. P. 1994, *PASP*, 106, 553
- Kraft, R. P., & Ivans, I. I. 2003, *PASP*, 115, 143
- Lehnert, M. D., Bell, R. A., & Cohen, J. G. 1991, *ApJ*, 367, 514
- Lee, Y.-W., Demarque, P., & Zinn, R. 1994, *ApJ*, 423, 248
- Lee, Y.-W., Gim, H. B., & Casetti-Dinescu, D. I. 2007, *ApJ*, 661, L49
- Lyons, M. A., Bates, B., Kemp, S. N., & Davies, R. D. 1995, *MNRAS*, 277, 113
- Marcolini, A., Gibson, B. K., Karakas, A. I., & Sánchez-Blázquez, P. 2009, *MNRAS*, 395, 719
- Marino, A. F., Milone, A. P., Piotto, G., Villanova, S., Bedin, L. R., Bellini, A., & Renzini, A. 2009, *A&A*, accepted for publication (arXiv:0905.4058v1)
- Monaco, L., Pancino, E., Ferraro, F. R., & Bellazzini, M. 2004, *MNRAS*, 349, 1278
- Norris, J. E., & Da Costa, G. S. 1995a, *ApJ*, 441, L81
- Norris, J. E., & Da Costa, G. S. 1995b, *ApJ*, 447, 680
- Norris, J., & Freeman, K. C. 1983, *ApJ*, 266, 130
- Norris, J. E., Freeman, K. C., & Mighell, K. J. 1996, *ApJ*, 462, 241
- Pancino, E., Pasquini, L., Hill, V., Ferraro, F. R., & Bellazzini, M. 2002, *ApJ*, 568, L101
- Piotto, G. 2009, *The Ages of Stars*, IAU Symposium 258, ed. E. E. Mamajek, D. R. Soderblom, & R. F. G. Wyse (Cambridge: CUP), 233 (arXiv:0902.1422v1)
- Romano, D., Matteucci, F., Tosi, M., Pancino, E., Bellazzini, M., Ferraro, F. R., Limongi, M., & Sollima, A. 2007, *MNRAS*, 376, 405
- Pritzl, B. J., Venn, K., & Irwin, M. 2005, *AJ*, 130, 2140
- Rutledge, G. A., Hesser, J. E., Stetson, P. B., Mateo, M., Simard, L., Bolte, M., Friel, E. D., & Copin, Y. 1997, *PASP*, 109, 883
- Rutledge, G. A., Hesser, J. E., & Stetson, P. B. 1997, *PASP*, 109, 907
- Sarajedini, A., & Layden, A. C. 1995, *AJ*, 109, 1086
- Smith, V. V., Suntzeff, N. B., Cunha, K., Gallino, R., Busso, M., Lambert, D. L., & Straniero, O. 2000, *AJ*, 119, 1239
- Stanford, L. M., Da Costa, G. S., Norris, J. E., & Cannon, R. D. 2006, *ApJ*, 647, 1075
- Stetson, P. B. 1987, *PASP*, 99, 191

Stetson, P. B. 1994, *PASP*, 106, 250

Zinn, R. 1993, *The Globular Cluster—Galaxy Connection* (ASP Conf. Ser. 48), ed. G. H. Smith & J. P. Brodie (San Francisco, CA: ASP), 38

Zinn, R., & West, M. J. 1984, *ApJS*, 55, 45